Mobility Increases the Surface Coverage of Distributed Sensor Networks

Xiao-Yang Liu[a*], Kai-Liang Wu[b], Yanmin Zhu[a], Linghe Kong[a], Min-You Wu[a]

[a]*Department of Computer Science and Engineering, Shanghai Jiao Tong University, Shanghai, China*

[b]*School of Mathematical Science, Peking University, Beijing, China*

Abstract

Coverage is a fundamental problem in sensor networks, which usually dictates the overall network performance. Previous studies on coverage issues mainly focused on sensor networks deployed on a 2D plane or in 3D space. However, in many real world applications, the target fields can be complex 3D surfaces where the existing coverage analysis methodology cannot be applied. This paper investigates the coverage of mobile sensor networks deployed over convex 3D surfaces. This setting is highly challenging because this dynamic type of coverage depends on not only sensors' movement but also the characteristics of the target field. Specifically, we have made three major contributions. First, we generalize the previous analysis of coverage in the 2D plane case. Second, we derive the coverage characterization for the sphere case. Finally, we next consider the general convex 3D surface case and derive the coverage ratio as a function of sensor mobility, sensor density and surface features. Our work timely fills the blank of coverage characterization for sensor networks and provides insights into the essence of the coverage hole problem. Numerical simulation and real-world evaluation verify our theoretical results. The results can serve as basic guidelines for mobile sensor network deployment in applications concerning complex sensing fields.

Keywords: Mobility, Surface Coverage, Distributed Sensor Networks

1. Introduction

Sensor networks are widely deployed in many commercial and military scenarios because of their unique advantages, such as low cost, ease of deployment and unattended operation. Typical applications include tracking wild animals [1][2], forest fire detection [3], forest carbon monitoring [4], volcano surveillance [5] and environmental data reconstruction [6][7].

Ensuring coverage is a fundamental problem in sensor networks and one of the main considerations for system designers [8]. The coverage of a sensor network answers important questions, e.g., what are the traces of the moving objects? What are the chances that an abnormal event like an intrusion will be detected during its lifetime? How well can the sensor network monitor a target field? How accurate is it if the sampled data are used to virtually reconstruct the environmental conditions of the field? Furthermore, the coverage property closely relates to the surveillance quality of a sensor network, the monitoring ability of an intrusion detection system and the connectivity of a k-hop clustered mobile wireless network [9]. Thus, it is important to understand the relationship between coverage and system parameters including the sensor density, sensors' mobility and field's properties. This will help designers better deploy sensor networks for various practical applications concerning complex sensing fields.

Recent years have witnessed the increasing adoption of mobile sensor networks. Sensors can be mounted on autonomous robots, such as the Pioneer 3DX [10] and the Starburg [11], or be mounted on wild animals [1][2]. System designers embrace mobile sensors since mobility enables self-deployment and adaptability. For example, in a hostile environment where sensors cannot be manually deployed, mobile sensors can move to the desired positions during the redeployment phase [12][13][14]; in ocean environments where sensors move with the surrounding ocean currents [11], mobile sensors can adapt to the floating water. Moreover, mobility can be exploited to compensate for the insufficient number of sensors, to improve the area coverage of a randomly deployed sensor network [18][19] and to optimize the data collection operation [6]. Recent studies have already shown that mobility can increase communication capacity [20], network connectivity [9] and security [21] in ad hoc networks.

1.1. Motivation

For the coverage characterization, most existing works assume that the target field is a 2D plane or 3D space. However, in many real world applications, the fields of interest ($FoIs$) are complex 3D surfaces (Fig 1(a)). Such examples appear in the ZebraNet project [1], the GreenOrbs project [4], and the Tungurahua volcano monitoring project [5]. In a 2D plane or 3D

*Corresponding author

Email addresses: yanglet@sjtu.edu.cn (Xiao-Yang Liu[a*]), wukl@pku.edu.cn (Kai-Liang Wu[b]), yzhu@sjtu.edu.cn (Yanmin Zhu[a]), linghe.kong@sjtu.edu.cn (Linghe Kong[a]), mwu@sjtu.edu.cn (Min-You Wu[a])

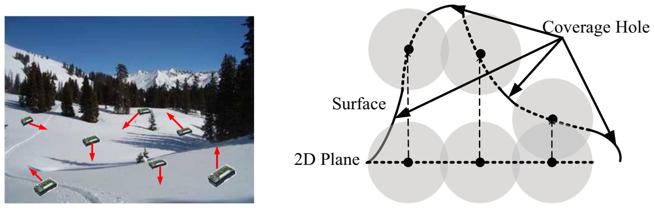

(a) (b)

Figure 1: a). An example of a mobile sensor network deployed over a 3D surface; b). A cross section view of **the coverage hole problem**: model the surface as a 2D plane, the deployment strategy that achieves full coverage on the 2D plane, however, will leave holes for the surface because sensors can only be positioned on the exposed area of the surface.

space, sensors can move freely within the whole FoI, but for 3D surfaces, sensors are restricted to move only on the surface. This implies that existing results derived under the 2D plane or 3D space model may be inappropriate when being applied to the 3D surface case.

Surface coverage is first introduced by M. Zhao *et al.* [22] and extended in [23]. They point out that coverage strategies derived on 2D planes do not work for 3D surfaces since they will encounter **the coverage hole problem** (Fig 1(b)). In [22][23], however, only surface coverage of static sensor networks is studied. The coverage ratio is determined by the initial network configuration and remains unchanged over time. B. Liu *et al.* [18] have analyzed the coverage of mobile sensor networks, but they concentrate on the 2D plane case and their results cannot be directly applied to the 3D surface case since their analysis fails to take into account the properties of the FoI. As a result, it is still not clear how mobility affects the coverage of mobile sensor networks on 3D surfaces.

To fill this gap, we study the surface coverage of a mobile sensor network deployed over a convex 3D surface. Specifically, we are interested in the surface coverage ratio over a time period, which is achieved by the continuous movement of sensors. Unlike traditional approaches that aim to provide simultaneous coverage of all locations at each time instant, or exploit mobility to obtain a new stationary configuration that improves the coverage ratio after the sensors move to the desired positions, the surface coverage in mobile scenarios aims at covering the locations once during an event's lifetime. This kind of surface coverage can be reduced to the scenario in [22][23] by making the sensors move at zero speed. Characterizing the surface coverage ratio of a mobile sensor network requires comprehensive consideration of the initial network configuration, features of the convex 3D surface and dynamic aspects of sensors' movement. In contrast, the stationary 2D plane coverage, mobile 2D plane coverage and stationary surface coverage consider only one or two of those three aspects.

1.2. Our Contributions

The main contributions in this paper are summarized as following:

- To the best of our knowledge, this is the first attempt at characterizing the surface coverage of distributed mobile sensor networks. We propose a theoretical analysis framework for coverage studies on general convex 3D surfaces.
- We derive theoretical results for 2D planes, spheres and general convex 3D surfaces under three mobility models. Our results show that mobility increases the surface coverage.
- Numerical simulation and real-world evaluation testify the accuracy of our theoretical results. Results using a 2D plane model perform poorly for 3D surfaces due to the coverage hole problem, which verifies our motivation.
- Our theoretical results provide insights into the essence of the coverage hole problem: the nonzero Gaussian curvature is the root cause for the invalidity of the 2D plane model for the surface coverage case.

The paper is organized as follows. Section 2 gives a brief review of related works, then in Section 3 we summarize our main results and give corresponding interpretations. The network model and coverage metrics are introduced in Section 4. Section 5 is devoted to consider the 2D plane case, while the sphere case is presented in Section 6. Section 7 shows our analysis framework for general surfaces, followed by our simulation and evaluation results in Section 8. In Section 9, we give a brief discussion, then conclude our work and point out possible directions for future work.

2. Related Works

Coverage of sensor networks has been extensively studied. Existing works on coverage can be divided into two categories: those focusing on stationary sensor networks and those focusing on mobile sensor networks. For the first class, various types of coverage have been investigated, such as area coverage [24][8][25][26], barrier coverage [27] and path coverage [28]. For the second class, two mobility models have been investigated: limited mobility [10][12][19][13][14], which assumes that the sensors can move only once over a short distance, and continuous mobility [11][18][29]. More thorough surveys on the coverage problem are provided by [28][30].

For stationary sensor networks, there are mainly four kinds of FoI models used: strip-shaped barrier, 3D space, 2D plane and 3D surface. Barrier coverage seeks to minimize the probability of undetected network penetrations [27]. 3D full space coverage [34][26] differs fundamentally from 3D complex surface coverage, because in the latter case sensors can only be deployed on the exposed surface area, not freely within the whole target FoI. For 2D plane coverage, Meguerdichian *et al.* [8] consider the coverage as a measure of the quality of service (QoS) of the sensor networks and design a robust, efficient, and scalable polynomial-time algorithm for connectivity and coverage based on Voronoi diagrams and Delaunay triangulations; P.-J. Wan and C.-W. Yi [24] address the asymptotic k-coverage of a randomly deployed sensor network. Still, proposed solutions under the 2D plane model have found a wide range of applications and some of them can be easily adapted to the 3D full space case. However, all of these results derived from the 2D plane and then applied to 3D complex surface, suffer from the coverage hole problem [22][23]. Thus, M.-C. Zhao *et al.* [22] propose using the concept of surface coverage and provide analytical results for the coverage ratio.

For mobile sensor networks, some work focuses on redeploying sensors to achieve a static configuration with better coverage. Based on potential fields, A. Howard *et al.* [12] model sensor nodes as virtual particles under the control of virtual forces. The virtual forces repel sensors away from each other and make sensors spread out, leading to a maximized coverage area. Y. Zou *et al.* [13] propose another virtual-force-based algorithm to improve the coverage of an initial randomly deployed sensor network and this virtual force is defined according to the distance between the sensor and the other sensors or obstacles. G. Wang *et al.* [14] propose several algorithms to identify coverage holes and compute the desired locations that can increase the coverage ratio the most. Those proposed algorithms strive to maximize the covered area in a redeployment phase which ends with sensors moving to form a new static configuration. The main difference is how exactly this new configuration is computed in an efficient manner.

Besides the work in [22][23], several recent papers also study the surface coverage problem. A distributed algorithm [15] is proposed to produce triangulations for arbitrary 3D surfaces. Further, [16] studies the optimal solution for 3D surface sensor deployment with minimized overall unreliability. It also designs a series of excellent algorithms for practical implementation. This study focused on sensor networks under the deterministic deployment. Liu *et al.* [17] derive the expected coverage ratio for irregular terrains using the cone/cos model and for irregular terrains using the digital elevation model. It focuses on sensor networks under the stochastic deployment. All of them target at stationary sensor networks.

B. Liu *et al.* [18] consider the coverage over an time interval resulting from the continuous movements of sensors, only on 2D planes. For 3D surfaces, the dynamic characteristics of the surface coverage of mobile sensor networks are left untouched. Our work fills the gap. We share a similar proof technique with [18], but the 3D surfaces are mathematically much more different and difficult compared with the 2D plane. Fortunately, the results in this paper are consistent with those on the static 2D plane case [24], the mobile 2D plane case [18] and the stationary 3D surface case [22]. This paper is the first to verify that the intuition introduced by [18] on the 2D plane also holds on the convex 3D surface: mobility increases the coverage of sensor networks.

3. Main Results

This section presents the main results and the corresponding implications. The notations are listed in TABLE 1, and readers can refer to it easily. Throughout the paper, $\|\cdot\|$ denotes the area of a region, or the arc length of a curve; $d(x_1, x_2)$ denotes the Euclidean distance between points x_1 and x_2; A' denotes the complement of set A. We define a function $\mathcal{G}_i(k_n, r, s)$ to characterize the properties of the FoI and the mobility of a sensor, with the following form:

Table 1: Notations

Symbol	Definition
S	The FoI, being a convex 3D surface or 2D plane.
C	The whole network or the locations of sensors.
s_i	The i^{th} sensor.
r	Sensing range.
λ	Network density.
v	Sensors' speed, being a constant.
K	Gaussian curvature of a surface.
t	A time instant in $[0, \tau)$.
$[0, \tau)$	The time interval of interest.
$[0, v\tau)$	The trace of a sensor over $[0, \tau)$.
$k(s)$	Curvature of a curve.
$k_g(s)$	Geodesic curvature at s.
$k_n(s)$	Normal curvature at s.
$\bar{k}_n(s)$	Conjugated normal curvature at s.
G_{c,s_i}, G^t_{c,s_i}	The region covered by s_i at t.
G_c, G^t_c	The *covered region* and *uncovered region* at t.
G^τ_{c,s_i}	The region covered by s_i over $[0, \tau)$.
G^τ_c	The covered region over $[0, \tau)$.
$f(t), F(\tau)$	Coverage ratio at t, over $[0, \tau)$.
$\mathcal{K}, \mathcal{U}$	Surface convex sets.

$$\mathcal{G}_i(k_n, r, s) = \frac{k_n(s)}{\bar{k}_n(s)}\left(r\sqrt{4-(\bar{k}_n(s)r)^2} + 4\,\frac{\bar{k}_n(s)-k_n(s)}{\bar{k}_n(s)k_n(s)}\arcsin\left(\frac{\bar{k}_n(s)r}{2}\right)\right). \quad (1)$$

Intuitively, $\mathcal{G}_i(k_n, r, s)$ indicates the local smoothness of the surface at the nearby region of point s. It quantitatively measures the bending degree of the surface area within the sensing range of a sensor node. $\mathcal{G}_i(k_n, r, s)$ has small value in sharp regions, and big value in smooth regions.

Our main theoretical results are:

- We generalize the results in the 2D plane case [18] by considering sensors moving along general curves. The expected area of the region covered by a mobile sensor s_i over the time period $[0, \tau)$ is $\|G^\tau_{c,s_i}\| = \pi r^2 + 2rv\tau$ as long as $r \le \min_{s\in[0,v\tau)} 1/k(s)$ when sensors move along straight lines (the SL Walk), circular arcs (the CA Walk) or general curves (the GC Walk). The coverage ratio, $F(\tau)$, is $1 - e^{-\lambda(\pi r^2+2rv\tau)}$.

- The coverage ratio of mobile sensor networks on a sphere is studied as a special case, i.e., a sphere is a convex 3D surface with constant Gaussian curvature K. The expected area of the region covered by a sensor s_i over the time period $[0, v\tau)$ is $\|G^\tau_{c,s_i}\| = \pi r^2 + rv\tau\sqrt{4 - Kr^2}$ as long as $r \le \sqrt{2(k-k_g)/(Kk)}$ under the CA Walk and the GC Walk, and $F(\tau) = 1 - e^{-\lambda[\pi r^2+rv\tau\sqrt{4-Kr^2}]}$, which gives us intuitions for the general surface case.

- We derive, in closed form, the coverage ratio on general convex 3D surfaces. We first identify that $\|G^\tau_{c,s_i}\| = \pi r^2 + \int_0^{v\tau}\mathcal{G}(k_n, r, s)ds + c(r)$ as long as $r \le$

$\min\limits_{s\in[0,v\tau)} \sqrt{2(k(s)-k_g(s))/(\overline{k}_n^2(s)k(s))}$ under the GC Walk; we then obtain a formula on the transformation from the area measure of G^{τ}_{c,s_i} to the coverage ratio; finally, let $h_r(v\tau) = \lim\limits_{n\to\infty} \frac{1}{n}\sum\limits_{i=1}^{n}\int_0^{v\tau}\mathcal{G}_i(k_n, r, s)ds$, if it exists, and then $F(\tau) = 1-e^{-\lambda[\pi r^2+h_r(v\tau)+c(r)]}$. $\mathcal{G}_i(k_n, r, s)$, defined in Equ(1), characterizes the properties of the FoI and the mobility of sensor, and the function $c(r)$ satisfies $\lim\limits_{r\to 0}\frac{c(r)}{r^3} = c, (|c| < \infty)$.

These results are consistent with previous results on the stationary 2D plane, mobile 2D plane and stationary surface scenarios [24][18][22]. We present the main implications of the above results below. From an abstract point of view, the first two reflect the inner consistency of our analysis methodology and thus verify the correctness of our results.

Remark 3.1. *For a sphere of radius R, $k_n(s) = \overline{k}_n(s) = \frac{1}{R}$, so we have*

$$\mathcal{G}_i(k_n, r, s) = r\sqrt{4-\left(\frac{r}{R}\right)^2} = r\sqrt{4-Kr^2},$$
$$h_r(v\tau) = rv\tau\sqrt{4-Kr^2},$$

and $c(r) = 0$ for the sphere case. Therefore, the coverage ratio of a sphere can be reduced from that in the general surface case:

$$F(\tau) = 1-e^{-\lambda[\pi r^2+h_r(v\tau)+c(r)]} = 1-e^{-\lambda[\pi r^2+rv\tau\sqrt{4-Kr^2}]}.$$

Remark 3.2. *When the sphere expands to a 2D plane, i.e. $R\to\infty$ $(K\to 0)$, then $h_r(v\tau) = \pi r^2 + 2rv\pi$. Therefore, the coverage ratio of the 2D plane can be reduced from these in both the sphere case and the general surface case.*

Remark 3.3. *The coverage ratio has the general form $F(\tau) = 1-e^{-\lambda[\pi r^2+h_r(v\tau)+c(r)]}$ for the mobility case, and $F(0) = 1-e^{-\lambda\pi r^2+c(r)}$ for the stationary case. Since $h_r(v\tau)$ is always positive, and $|c(r)|$ is smaller than $h_r(v\tau)$, so*

$$F(\tau) = 1-e^{-\lambda[\pi r^2+h_r(v\tau)+c(r)]} \geq 1-e^{-\lambda\pi r^2} = F(0).$$

Then we always have that mobility increases the surface coverage of sensor networks. Furthermore, since $h_r(v\tau)$ increases with $v\tau$, there are two ways for increasing $F(\tau)$: increasing the sensors' moving speed or prolonging the time interval.

Remark 3.4. *From function $h_r(v\tau)$ and $\mathcal{G}(k_n, r, s)$, we know that sensors moving at positions with bigger Gaussian curvature will cover a region with less area. It is not difficult to check that the inequality $\mathcal{G}(k_n, r, s)\leq 2r$ always holds, with equality holding for the 2D plane case. Therefore, given the speed, the area covered by sensors moving on a 2D plane over an equivalent time interval is larger than that on general 3D surfaces. This lead us to the conclusion that the nonzero Gaussian curvature leads to the invalidity of the 2D plane model for 3D surfaces, i.e., the coverage hole problem.*

4. Network Models and Metrics

This section describes models for FoI, sensing, deployment and mobility pattern, respectively, and presents several measures to assess the surface coverage performance of mobile sensor networks.

To understand our work, the reader must be familiar with preliminaries of the integral and differential geometry theories. For convenience, Appendix A lists the related definitions and theorems.

4.1. The Unit Ball Sensing Model

We assume that the target FoI is a convex surface S of class $\mathbb{C}^2$ in 3D space[1]. S can be expressed as a single valued function $z = h(x, y)$ in a Cartesian coordinate system. In particular, S is a *plane* if and only if the function is $z = c$ where c is a constant, for an appropriate selection of the coordinate system. A sensor s_i is said to be placed on S if the coordinates of s_i satisfy the equation of S, which is denoted as $s_i \in S$.

We use a unit ball sensing model, i.e., assume that each sensor has the same sensing radius r in 3D Euclidean space and that a sensor can sense and detect events within its sensing range[2], thus the sensing region forms a ball of radius r centered at s_i in 3D space (or a disk on a 2D plane).

Let G_{c,s_i} denote the region covered by sensor s_i on S, we have $G_{c,s_i} \subseteq S$ with

$$G_{c,s_i} = \{x \mid d(s_i, x) \leq r, x\in S\}. \tag{2}$$

A point $p\in S$ is said to be *covered* by sensor s_i if $p\in G_{c,s_i}$. After n sensors are deployed, the FoI is thus partitioned into two kinds of regions: the *covered region* G_c and the *uncovered region* G'_c:

$$G_c = \bigcup_{i=1}^{n} G_{c,s_i}. \tag{3}$$

Every point in G_c is covered by at least one sensor; G'_c is the complement of G_c. An event happening in G_c or an intruder appearing in this region will be detected immediately.

4.2. Sensor Deployment

Definition 4.1. *Surface Poisson Point Process (SP3). Assume that sensors are distributed uniformly, both $n, \|S\|\to\infty$ in such a way that $\frac{n}{\|S\|}\to\lambda$ (which is a positive constant), the probability that there are m sensors lie in a set G is*

$$\lim_{\substack{n\to\infty\\ \|S\|\to\infty}} \frac{(\lambda\|G\|)^m}{m!}e^{-\lambda\|G\|}. \tag{4}$$

The right-hand side of Equ.(4) is the probability function of the Poisson distribution; it depends only on the product $\lambda\|G\|$,

[1] Convex surface, Gaussian curvature, surface of class $\mathbb{C}^k$ are considered as a prior knowledge. Refer to Appendix A or [31] for detailed definitions.

[2] This assumption is a bit strong but quite satisfying as S is quite large and r is small in real world scenarios; it simplifies the analysis a lot. Refer to Section 9 for further discussions.

which is called the parameter of the distribution. This probability model for points on the surface is said to be a Surface Poisson Point Process (SP3) of intensity λ. Note that λ is the network density.

We concentrate on large-scale mobile sensor networks deployed over vast 3D surfaces[3]. For the initial configuration, we assume that the locations of these sensors are uniformly and independently distributed according to the $SP3$ model at time $t = 0$, as in [22][23].

We adopt the Surface Poisson Point Process ($SP3$) due to the following two reasons: (1) $SP3$ provides a uniform distribution for the initial locations of sensors; (2) If sensors move by choosing its forwarding directions independently and randomly, $SP3$ holds in the whole process. This uniform property simplifies our analysis greatly and we believe that it might serve as a basis for analyzing other kinds of distribution patterns, since many more complicated distributions can be reduced to uniform distributions as Gaussian distribution and exponential distribution giving proper parameters.

4.3. Mobility Model

In this work, we consider the following three simple sensor mobility models: SL Walk, CA Walk and GC Walk. The movement of a sensor is characterized by its speed and direction. We assume that sensors move independently of each other, as in [18]. All sensors move with constant velocity v. Ignoring the edge effect as S is vast or infinite, then the $SP3$ distribution always holds during time interval $[0, \tau)$.

- **Straight line walk (SL Walk)**: On 2D planes, each sensor randomly chooses a direction from $[0, 2\pi)$ uniformly at $t = 0$ and never change over $[0, \tau)$. It is quite similar to the **Random Waypoint Model**.
- **Circular arc walk (CA Walk)**: On 2D planes/spherical surfaces, each sensor randomly chooses a direction $\alpha \in [0, 2\pi)$ uniformly at $t = 0$ and then performs **uniform circular motion** with radius of $1/k$.
- **General curve walk (GC Walk)**: Divide time into appropriate slots. On 2D planes/sphere/general surfaces, each sensor randomly chooses a direction form all possible directions uniformly at the beginning of each slot and then move forward with constant velocity v.

The SL and CA Walk are special cases of the GC Walk, and the results of the SL and CA Walk are intermediate results for the proof of the GC Walk case. More specifically, in the 2D plane case, sensors can perform straight line walk, circular arc walk and general curve walk; in the sphere case, sensors can perform circular arc walk and general curve walk; while in the general convex 3D surface case, sensors can perform only general curve walk. Furthermore, the results obtained on 2D planes and 3D spheres are then extended to the general convex 3D surfaces; the results of straight line walk are extended to derive results for the circular arc walk, then for the general curve walk.

These above random mobility models enable us to prove the final argument that "Mobility increased the surface coverage of distributed sensor networks", because even this simply and naive motion ability increases the network performance greatly, then elaborate, intelligent and collective mobility is bound to promote network performance more. This methodology is also adopted by [20][9][21][18], which assume random mobility model to prove that mobility increases communication capacity, network connectivity, security and 2D coverage, respectively.

4.4. Coverage Metrics

In [22][23], the authors consider the full surface coverage in stationary scenario, which can be formally defined as: find a deployment strategy using the minimum number of sensors while providing full coverage of the FoI. Here, we take a different approach and establish a theoretical analysis framework for partial surface coverage by characterizing the coverage ratio, i.e., studying how initial network configuration, properties of the surface and mobility pattern together affect the coverage ratio.

To study the surface coverage, we use the following three coverage measures: area coverage ratio at time instant t, $f(t)$, the area covered by one sensor s_i over a time interval $[0, \tau)$, $\|G^{\tau}_{c,s_i}\|$, and area coverage ratio over $[0, \tau)$, $F(\tau)$. Let G^t_c denote the *covered region* of the FoI at t and G^{τ}_c denote the region covered over $[0, \tau)$, which is defined by

$$\left\|G^{\tau}_{c,s_i}\right\| = \Big\| \bigcup_{t\in[0,\tau)} G^t_{c,s_i} \Big\|, \qquad \left\|G^{\tau}_c\right\| = \Big\| \bigcup_{i=1}^{n} G^{\tau}_{c,s_i} \Big\|. \tag{5}$$

Area coverage ratio at t is defined by the probability that a randomly selected point from S lies in G^t_c, i.e. $\mathcal{P}\left(p \in G^t_c \mid p \in S\right)$, as both $n, \|S\| \to \infty$ in such a way that $\frac{n}{\|S\|} \to \lambda$, if the following limit

$$f(t) = \lim_{\substack{n\to\infty \\ \|S\|\to\infty}} \mathcal{P}\left(p \in G^t_c \mid p \in S\right) \tag{6}$$

exists, then $f(t)$ is the corresponding coverage ratio. Similarly, we define $F(\tau)$ as

$$F(\tau) = \lim_{\substack{n\to\infty \\ \|S\|\to\infty}} \mathcal{P}\left(p \in G^{\tau}_c \mid p \in S\right). \tag{7}$$

All three coverage measures depend not only on the network configuration, but also on the sensor mobility pattern. $f(t)$ is the fraction of the geographical area covered by at least one sensor at time instant t; it measures the coverage ratio achieved by a sensor network at a snapshot view. Specifically, for a stationary scenario, $f(t)$ remains unchanged, i.e., $f(t) = f(0), \forall t \in [0, \tau)$, and mainly depends on the network's initial configuration (e.g., the sensor distribution, network density and sensing range) and the properties of the FoI. Since our networks are homogeneous

[3]We concentrate on large-scale homogeneous mobile sensor networks: Large-scale is reflected in both the number of sensors and the area of the FoI are infinite (as $n, \|S\| \to \infty$); homogeneous means that the capability of the sensors are the same, and that the sensors are distributed uniformly, e.g. deploying sensors by vehicles running on the surface or even by aircraft, humans and robots.

and sensors move under an identical random and independent way on surface, the expectation of the area covered during any given time period by each sensor is the same. Thus without loss of generality, we denote it by a common symbol, as G^t_{c,s_1} for G^t_{c,s_i}, G^τ_{c,s_1} for G^τ_{c,s_i}, $\forall i \in [2, n]$. $F(\tau)$ measures the area coverage ratio of a mobile sensor network during the time interval $[0, \tau)$, which is the fraction of the geographical area covered by at least one sensor at least once at some time instant t. As pointed out by B. Liu *et al* [18], the characterization of area coverage ratio at specific time instant is useful for applications that require simultaneous coverage, while the area coverage ratio over a time interval is appropriate for applications that do not require simultaneous coverage of all positions at specific time instant, but rather prefer partial-time coverage.

5. Mobility on a 2D Plane

The 2D plane is a special case of complex surface with Gaussian curvature of zero. The results seem to be straightforward, but can provide a brief overview of the proving process in the following sections. B. Liu *et al.* [18] discussed the situation where sensors move under the SL Walk. In this section, we further study the area coverage achieved under the CA and GC Walk. As the SL and CA Walk are special cases of the GC Walk, we thus generalize the results of [18].

Lemma 5.1. *The SP3 distribution model can be reduced to the Poisson Point Process (PP3) on a 2D plane.*

Proof. For a 2D plane, the Gaussian curvature of S is zero. Combining Definition 4.1 and Lemma Appendix A.4, it can be immediately obtained. □

Theorem 5.2. *Consider the mobile sensor network, C, deployed under the SP3 model on plane S at time instant $t_0 = 0$. Sensors move under the SL, SA and GC Walk over $[0, \tau)$. If $r \le \min_{s\in[o,v\tau)} 1/k(s)$, then we have:*

$$f(t) = 1 - e^{-\lambda\pi r^2}, \forall t \in [0, \tau),$$
$$||G^\tau_c|| = \pi r^2 + 2rv\tau,$$
$$F(\tau) = 1 - e^{-\lambda(\pi r^2 + 2rv\tau)}.$$

Proof. For the SL walk, shown in Fig 2(a), the results were presented in [18]. They hold because under the SL Walk, at each time instant $t \in [0, \tau)$, the locations of the sensors still follow the Poisson Point Process (PP3) of the same density [32]. Next we study the CA and GC Walk during $[0, \tau)$.

1) The CA Walk is shown in Fig 2(b). The covered region forms a circular race track with radius R. G^τ_{c,s_i}, which is the initial covered region plus the region covered by the diameter of the sensor, has the area:

$$\begin{aligned}\left\|G^\tau_{c,s_i}\right\| &= \pi r^2 + \frac{R\theta}{2\pi R} \cdot \pi[(R+r)^2 - (R-r)^2] \\ &= \pi r^2 + \frac{v\tau}{2\pi R} \cdot 4\pi R r = \pi r^2 + 2rv\tau.\end{aligned} \tag{8}$$

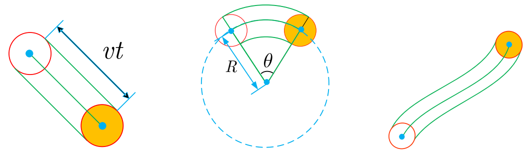

Figure 2: Sensor moves on a 2D plane. (a). The SL Walk case; (b). The CA Walk case; (c). The GC Walk case.

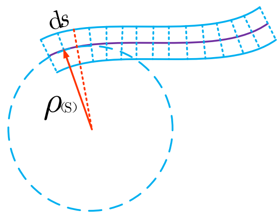

Figure 3: The infinitesimal dividing method in the GC Walk case.

2) The GC Walk is shown in Fig 2(c). The covered region has a curly ring shape. Denote the curve as $\mathcal{L}(s), (0 \le s < v\tau)$ and the radius at s as $\rho(s) = 1/k(s)$. Let $r \le \min_{s\in[0,v\tau)} 1/k(s)$. The infinitesimal arc element $[s, s + ds]$ (see Fig 3) can be approximated by an elementary circular arc with radius of $\rho(s)$. The expected area covered by the diameter of a sensor moving along $[s, s + ds]$ is $dS = 2rds$. By integration, we get:

$$\begin{aligned}\left\|G^\tau_{c,s_i}\right\| &= \pi r^2 + \int_{\mathcal{L}(s)} dS = \pi r^2 + \int_0^{v\tau} 2rds \\ &= \pi r^2 + 2rv\tau.\end{aligned} \tag{9}$$

3) It was pointed out in [33] that area coverage ratio depends on the distribution of the random shapes only through its expected area measure, thus we have:

$$F(\tau) = 1 - e^{-\lambda\|G^\tau_{c,s_i}\|} = 1 - e^{-\lambda(\pi r^2 + 2rv\tau)}. \tag{10}$$

□

6. Mobility on a Sphere

A sphere is another special case of 3D surfaces. A sphere with radius R has constant Gaussian curvature $K = 1/R^2$. In this section, we study the scenario when sensors move under the CA and GC Walk.

Lemma 6.1. *On a sphere of radius R, the geodesic curvature k_g of a circular arc curve with radius ρ satisfies:*

$$k_g = \pm\frac{\sqrt{R^2 - \rho^2}}{R\rho}. \tag{11}$$

Proof. From Lemma Appendix A.1, and $k_n = 1/R$, we have:

$$k_g = \pm\sqrt{k^2 - k_n^2} = \pm\sqrt{\frac{1}{\rho^2} - \frac{1}{R^2}} = \pm\frac{\sqrt{R^2 - \rho^2}}{R\rho}.$$

The sign is determined by the projection direction of the curve on it tangent plane: if the projection directs to the inner of the region, it is positive; otherwise, it is negative. □

Theorem 6.2. *Consider the mobile sensor network, C, deployed under the SP3 model on sphere S at time instant $t_0 = 0$. Sensors move under the CA Walk over $[0, \tau)$; s_i moves along a circular arc of curvature k. We have:*

$$\left\|G^{\tau}_{c,s_i}\right\| = \pi r^2 + rv\tau\sqrt{4 - Kr^2},$$

if $r \le \sqrt{\frac{2(k-k_g)}{Kk}}$.

Refer to the appendix for the corresponding proof.

Remark 6.1. *For the CA Walk, the proving process assumes that the sensing range is relatively small, such that*

$$r \le \|DC\| = \sqrt{\rho^2 + \left(R - \sqrt{R^2 - \rho^2}\right)^2} = \sqrt{\frac{2(k - k_g)}{Kk}}.$$

Remark 6.2. *For the CA Walk, letting $\tau \to 0$, we get the result for stationary network scenarios:*

$$\left\|G^{0}_{c,s_i}\right\| = \lim_{\tau\to 0} G^{\tau}_{c,s_i} = \lim_{\tau\to 0}\left(\pi r^2 + rv\tau\sqrt{4 - Kr^2}\right) = \pi r^2.$$

Remark 6.3. *For the CA Walk, over $[0, \tau)$, let Ω_{c,s_i} denote the additional region covered by the diameter of sensor s_i due to its movement, then*

$$\left\|\Omega_{c,s_i}\right\| = \left\|G^{\tau}_{c,s_i}\right\| - \left\|G^{0}_{c,s_i}\right\| = rv\tau\sqrt{4 - Kr^2}.$$

This indicates that on spherical surface, at each snapshot, the area covered by a sensor is constant as long as $r \le \sqrt{2(k - k_g)/(Kk)}$. Furthermore, as long as this condition holds along the moving trace, the expected area covered by the mobile sensor over $[0, \tau)$ is independent of the trajectory.

Theorem 6.3. *Consider the mobile sensor network C deployed under the SP3 model on sphere S at time instant $t_0 = 0$. Sensors move under GC Walk; s_i moves along a general curve of curvature $k(s)$, $0 \le s < v\tau$. We have*

$$\left\|G^{\tau}_{c,s_i}\right\| = \pi r^2 + rv\tau\sqrt{4 - Kr^2},$$

if $r \le \min\limits_{0\le s<v\tau}\left(\sqrt{\frac{2(k(s)-k_g(s))}{Kk(s)}}\right)$.

Proof. By utilizing a similar methodology as in the 2D plane case, for the GC Walk, we approximate the infinitesimal arc element dS as an elementary circular arc; by integration we obtain the final result.

Denote the curve as $\mathcal{L}(s), 0 \le s < v\tau$, and the radius at s is $\rho(s) = 1/k(s)$. For a infinitesimal element $[s, s + ds]$, which can be approximated as an elementary circular arc with radius of $\rho(s)$, from Remark 6.3, we know that the area covered by the diameter of a sensor moving along $[s, s + ds]$ is $dS = r\sqrt{4 - Kr^2}ds$. By integration, we get

$$\left\|\Omega^{\tau}_{c,s_i}\right\| = \int_{\mathcal{L}(s)} dS = \int_0^{v\tau} r\sqrt{4 - Kr^2}ds = rv\tau\sqrt{4 - Kr^2}, \tag{12}$$

$$\left\|G^{\tau}_{c,s_i}\right\| = \left\|\Omega^{\tau}_{c,s_i}\right\| + \left\|G^{0}_{c,s_i}\right\| = \pi r^2 + rv\tau\sqrt{4 - Kr^2}. \tag{13}$$

□

Theorem 6.4. *Consider the mobile sensor network, C, deployed under the SP3 model on S at time instant $t_0 = 0$. Sensors move under the GC Walk and along general curves $\mathcal{L}(s)$, $0 \le s < v\tau$ over $[0, \tau)$. We have*

$$\mathcal{P}\left(p \in \bigcup_{i=1}^{n} G^{\tau}_{c,s_i} \mid p \in S\right) = 1 - \left(1 - \frac{\pi r^2 + rv\tau\sqrt{4 - Kr^2}}{4\pi/K}\right)^n,$$

$$F(\tau) = 1 - e^{-\lambda(\pi r^2 + rv\tau\sqrt{4-Kr^2})},$$

if $r \le \min\limits_{0\le s<v\tau}\left(\sqrt{\frac{2(k(s)-k_g(s))}{Kk(s)}}\right)$.

Proof. From Theorem 6.3, we know that $\left\|G^{\tau}_{c,s_i}\right\| = \pi r^2 + rv\tau\sqrt{4 - Kr^2}$. Since the FoI is the entire spherical surface S with $\|S\| = 4\pi R^2 = \frac{4\pi}{K}$ and $G^{\tau}_{c,s_i} \subseteq S$, the probability that a random chosen point $p \in S$ lies in G^{τ}_{c,s_i} is

$$\mathcal{P}\left(p \in G^{\tau}_{c,s_i}\right) = \frac{\left\|G^{\tau}_{c,s_i}\right\|}{\|S\|} = \frac{\pi r^2 + rv\tau\sqrt{4 - Kr^2}}{4\pi/K}. \tag{14}$$

Because each sensor moves independently, thus we get

$$\begin{aligned}
\mathcal{P}\left(p \in \bigcup_{i=1}^{n} G^{\tau}_{c,s_i}\right) &= 1 - \mathcal{P}\left(p \in \left(\bigcup_{i=1}^{n} G^{\tau}_{c,s_i}\right)'\right) \\
&= 1 - \mathcal{P}\left(p \in \bigcap_{i=1}^{n}\left(G^{\tau}_{c,s_i}\right)'\right) = 1 - \prod_{i=1}^{n}\mathcal{P}\left(p \in \left(G^{\tau}_{c,s_i}\right)'\right) \\
&= 1 - \prod_{i=1}^{n}\left[1 - \mathcal{P}\left(p \in G^{\tau}_{c,s_i}\right)\right] \\
&= 1 - \left(1 - \frac{\pi r^2 + rv\tau\sqrt{4 - Kr^2}}{4\pi/K}\right)^n.
\end{aligned} \tag{15}$$

Note that $\left(1 - \frac{1}{x}\right)^x \xrightarrow{x\to\infty} e^{-1}$, $\frac{n}{\|S\|} = \lambda$, thus

$$\begin{aligned}
F(\tau) &= \lim_{\substack{n\to\infty \\ \|S\|\to\infty}} \mathcal{P}\left(p \in \bigcup_{i=1}^{n} G^{\tau}_{c,s_i} \mid p \in S\right) \\
&= \lim_{\substack{n\to\infty \\ \|S\|\to\infty}}\left[1 - \left(1 - \lambda\cdot\frac{\pi r^2 + rv\tau\sqrt{4 - Kr^2}}{n}\right)^n\right] \\
&= 1 - e^{-\lambda(\pi r^2 + rv\tau\sqrt{4-Kr^2})}.
\end{aligned} \tag{16}$$

□

7. Mobility on a General Convex 3D Surface

This section is devoted to analyzing the surface coverage ratio on general surfaces when sensors move under the GC Walk. We follow a similar methodology as in the 2D plane case and the sphere cases, but is much more complicated. First we study the diameter and area of the region covered by a moving sensor;

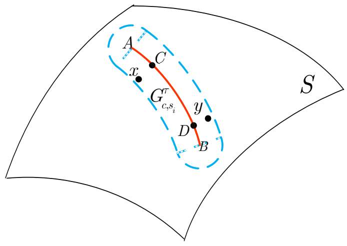

Figure 4: Diameter of the region covered by a moving sensor s_i.

then characterize the probability of the following event: a random chosen point from a surface convex set lies in a subset of that set; finally we are able to obtain the formula of $F(\tau)$ with full consideration of the initial sensor distribution, properties of the target surface field and mobility pattern of sensors.

Lemma 7.1. *On a general surface, let G^{τ}_{c,s_i} be the region covered by a moving sensor over $[0,\tau)$, and $|G^{\tau}_{c,s_i}|_D$ be the diameter of G^{τ}_{c,s_i}. We have*

$$|G^{\tau}_{c,s_i}|_D \leq 2r + v\tau.$$

Proof. Randomly pick two points x,y from G^{τ}_{c,s_i}, as shown in Fig 4. Let $\widehat{AB}$ denote the trace of sensor s_i. According to the definition of G^{τ}_{c,s_i}, we know that $\exists$ points $C, D \in \widehat{AB}$, *s.t.* $x \in \overline{B(C,r)} \cap S$, $y \in \overline{B(D,r)} \cap S$, where $\overline{B(C,r)}$ denote a ball with radius r and center point C. Then the following inequality holds:

$$\begin{aligned} d(x,y) &\leq d(x,C) + d(C,D) + d(D,y) \\ &\leq r + \|\widehat{CD}\| + r \ \leq 2r + \|\widehat{AB}\| \leq 2r + v\tau. \end{aligned} \tag{17}$$

Therefore, $\left|G^{\tau}_{c,s_i}\right|_D = \sup_{\forall x,y \in G^{\tau}_{c,s_i}} \left\{ d(x,y) \right\} \leq 2r + v\tau.$ □

Theorem 7.2. *Consider the mobile sensor network, C, deployed under SP3 model on S at time instant $t_0 = 0$. If sensors move under the GC Walk; sensor i is assumed to move along general curve of curvature $k(s)$, $0 \leq s < v\tau$. We have*

$$\left\|G^{\tau}_{c,s_i}\right\| = \pi r^2 + \int_0^{v\tau} \mathcal{G}_i(k_n, r, s)ds + c(r)$$

if $r \leq \min_{0 \leq s < v\tau} \left(\sqrt{\frac{2(k(s)-k_g(s))}{\overline{k}_n^2(s)k(s)}} \right)$,
where the function $c(r)$ satisfies $\lim_{r\to 0} \frac{c(r)}{r^3} = c$, $(|c| < \infty)$, and $\mathcal{G}_i(k_n, r, s)$ characterizes the properties of the surface and mobility pattern of sensor i, with the following form:

$$\begin{aligned} &\mathcal{G}_i(k_n, r, s) \\ &= \frac{k_n(s)}{\overline{k}_n(s)} \left(r\sqrt{4 - (\overline{k}_n(s)r)^2} + 4\,\frac{\overline{k}_n(s) - k_n(s)}{\overline{k}_n(s)k_n(s)} \arcsin\left(\frac{\overline{k}_n(s)r}{2}\right) \right). \end{aligned}$$

Refer to the appendix for the corresponding proof.

Given sensing range r and the target FoI, $\mathcal{G}(k_n, r, s)$ depends only on the trace of each sensor. So we call $\mathcal{G}(k_n, r, s)$ the mobility function, which characterizes sensor's mobility.

Remark 7.1. *There are two special cases we would like to point out. If $\overline{k}_n(s) = 0$, the mobility function can be obtained by taking the limit, i.e., $\mathcal{G}_i(k_n, r, s) = 2r$; If $\overline{k}_n(s) \neq 0$ and $k_n(s) = 0$, it can also be obtained by taking the limit, i.e., $\mathcal{G}_i(k_n, r, s) = \frac{4}{\overline{k}_n(s)} \arcsin\left(\frac{\overline{k}_n(s)r}{2}\right)$.*

Next, we characterize the coverage ratio over a time interval $[0, \tau)$. First, we need establish the random process on general surface, which is mathematically hard due to the lack of existing theoretical results. We utilize the rules of clipping and approaching, which can produce satisfactory results for our analysis.

Theorem 7.3. *Consider a general convex surface $S : z = h(x,y)$, which satisfies $\max_S \|\bigtriangledown h\| < \infty$, and a surface convex set $\mathcal{U}$. Randomly pick a surface convex set $\mathcal{K} \subseteq S$ such that $\mathcal{U} \cap \mathcal{K} \neq \emptyset$, the probability that a randomly selected point in $\mathcal{U}$ is also located in $\mathcal{K}$ is given by*

$$\mathcal{P}(p \in \mathcal{U} \cap \mathcal{K} | \mathcal{U} \cap \mathcal{K} \neq \emptyset) = \frac{\mathcal{K}}{\mathcal{U} + \xi(\mathcal{U}, \mathcal{K})}$$

with the function $\xi(\mathcal{U}, \mathcal{K})$ satisfies

$$0 \leq \xi(\mathcal{U}, \mathcal{K}) \leq M(\|\partial \mathcal{U}'\|\delta + \pi\delta^2),$$

where $M = \max_S \sqrt{1 + \|\bigtriangledown h\|^2}$, and $\delta = \sup_{\mathcal{K} \subseteq S} |K|_D$, $\mathcal{U}_z$ denotes the z-projection of $\mathcal{U}$ on the plane xOy.

Refer to the appendix for the corresponding proof.

Theorem 7.4. *Consider a general infinite convex surface $S : z = h(x,y)$ satisfying[4] $\max_S \|\bigtriangledown h\| < \infty$, and assume that sensors move under the GC Walk over $[0,\tau)$. Let $h_r(v\tau) = \lim_{n\to\infty} \frac{1}{n} \sum_{i=1}^{n} \int_0^{v\tau} \mathcal{G}_i(k_n, r, s)ds$, we have*

$$\lim_{n\to\infty} \mathcal{P}\left(p \in \bigcup_{1 \leq i \leq n} G^{\tau}_{c,s_i}\right) \to 1 - e^{-\lambda[\pi r^2 + h_r(v\tau) + c(r)]}$$

if $r \leq \min_{s \in [0, v\tau)} \sqrt{\frac{2(k(s)-k_g(s))}{\overline{k}_n^2(s)k(s)}}$, or equivalently,

$$F(\tau) = 1 - e^{-\lambda[\pi r^2 + h_r(v\tau) + c(r)]},$$

where $\mathcal{G}_i(k_n, r, s)$ characterizes the properties of the FoI and the mobility of sensor i, and the function $c(r)$ satisfies $\lim_{r\to 0} \frac{c(r)}{r^3} = c$, $(|c| < \infty)$.

Proof. As pointed out in Theorem 7.2 and Theorem 7.3, the area measure of the region covered by sensor s_i over $[0,\tau)$ is $\left\|G^{\tau}_{c,s_i}\right\|$ and the probability that a random chosen point on S lies in this region is $\mathcal{P}(p \in G^{\tau}_{c,s_i})$, as:

$$\left\|G^{\tau}_{c,s_i}\right\| = \pi r^2 + \int_0^{v\tau} \mathcal{G}_i(k_n, r, s)ds + c(r), \tag{18}$$

[4] Intuitively, this condition assures that the surface S has no sudden change.

$$\mathcal{P}(p \in G^{\tau}_{c,s_i}) = \frac{\left\|G^{\tau}_{c,s_i}\right\|}{\|S\| + \xi(S, G^{\tau}_{c,s_i})}, \tag{19}$$

with $\xi(\mathcal{S}, G^{\tau}_{c,s_i})$ satisfies

$$0 \le \xi(S, G^{\tau}_{c,s_i}) \le M(\|\partial S_z\|\delta_{s_i} + \pi\delta^2_{s_i}), \tag{20}$$

$$0 \le \frac{\xi(S, G^{\tau}_{c,s_i})}{\|S\|} \le \frac{M(\|\partial S_z\|d + \pi d^2)}{\|S\|} \xrightarrow{\|S_z\|\to\infty} 0. \tag{21}$$

Then, we have

$$\mathcal{P}(p \in \bigcup_{1\le i\le n} G^{\tau}_{c,s_i}) = 1 - \prod_{1\le i\le n}\left[1 - \mathcal{P}(p \in G^{\tau}_{c,s_i})\right]$$
$$= 1 - \prod_{1\le i\le n}\left[1 - \frac{\left\|G^{\tau}_{c,s_i}\right\|}{\|S\| + \xi(S, G^{\tau}_{c,s_i})}\right] = 1 - \prod_{1\le i\le n}\left(1 - \frac{\beta_i}{n}\right), \tag{22}$$

where

$$\beta_i = \frac{n\left\|G^{\tau}_{c,s_i}\right\|}{\|S\| + \xi(S, G^{\tau}_{c,s_i})} \xrightarrow{n\to\infty} \lambda\left\|G^{\tau}_{c,s_i}\right\|. \tag{23}$$

Note that the following relations hold:

$$\lim_{n\to\infty,\|S\|\to\infty} \frac{n}{\|S\|} = \lambda, \quad \lim_{n\to\infty,\|S\|\to\infty} \frac{\xi(S, G^{\tau}_{c,s_i})}{\|S\|} = 0. \tag{24}$$

Since $h_r(v\tau) = \lim_{n\to\infty} \frac{1}{n}\sum_{i=1}^{n} \int_0^{v\tau} \mathcal{G}(k_n, r, s)ds$, we get

$$\lim_{n\to\infty} \frac{1}{n}\sum_{i=1}^{n} \beta_i = \lambda \lim_{n\to\infty} \frac{1}{n}\sum_{i=1}^{n} \|G^{\tau}_{c,s_i}\| = \lambda\left[\pi r^2 + h_r(v\tau) + c(r)\right], \tag{25}$$

$$\lim_{n\to\infty} \frac{1}{\|S\| - \|G^{\tau}_{c,s_i}\|}\sum_{i=1}^{n} \|G^{\tau}_{c,s_i}\| = \lim_{n\to\infty} \frac{\|S\|}{\|S\| - \|G^{\tau}_{c,s_i}\|}\frac{n}{\|S\|}\frac{1}{n}\sum_{i=1}^{n} \|G^{\tau}_{c,s_i}\|$$
$$= \lambda\left[\pi r^2 + h_r(v\tau) + c(r)\right]. \tag{26}$$

Therefore, for $\forall\epsilon > 0$, we obtain the following relations as $n \to \infty$:

$$\prod_{1\le i\le n}\left(1 - \frac{\beta_i}{n}\right) \le \left[1 - \frac{1}{n}\left(\frac{1}{n}\sum_{i=1}^{n}\beta_i\right)\right]^n$$
$$\le \left[1 - \frac{1}{n}\left(\lambda\left[\pi r^2 + h_r(v\tau) + c(r)\right] - \epsilon\right)\right]^n \tag{27}$$
$$\xrightarrow{n\to\infty} e^{-\lambda\left[\pi r^2 + h_r(v\tau) + c(r)\right] + \epsilon},$$

$$\prod_{1\le i\le n}\left[1 - \frac{\left\|G^{\tau}_{c,s_i}\right\|}{\|S\| + \xi(S, G^{\tau}_{c,s_i})}\right] \ge \prod_{1\le i\le n}\left(1 - \frac{\left\|G^{\tau}_{c,s_i}\right\|}{\|S\|}\right)$$
$$= \left[\prod_{1\le i\le n}\left(1 + \frac{\left\|G^{\tau}_{c,s_i}\right\|}{\|S\| - \left\|G^{\tau}_{c,s_i}\right\|}\right)\right]^{-1}$$
$$\ge \left[\frac{1}{n}\sum_{i=1}^{n}\left(1 + \frac{\left\|G^{\tau}_{c,s_i}\right\|}{\|S\| - \left\|G^{\tau}_{c,s_i}\right\|}\right)\right]^{-n} \tag{28}$$
$$= \left[1 + \frac{1}{n}\frac{\|S\|}{\|S\| - \|G^{T}_{c,s_i}\|}\frac{1}{\|S\|}\sum_{i=1}^{n}\|G^{\tau}_{c,s_i}\|\right]^{-n}$$
$$\ge \left[1 + \frac{\lambda\left[\pi r^2 + h_r(v\tau) + c(r)\right] + \epsilon}{n}\right]^{-n}$$
$$\xrightarrow{n\to\infty} e^{-\lambda\left[\pi r^2 + h_r(v\tau) + c(r)\right] - \epsilon}.$$

Hence, we get

$$F(\tau) = \lim_{n\to\infty} \mathcal{P}\left(p \in \bigcup_{1\le i\le n} G^{\tau}_{c,s_i}\right) = 1 - e^{-\lambda[\pi r^2 + h_r(v\tau) + c(r)]}, \tag{29}$$

where $c(r)$ satisfies $\lim_{r\to 0} \frac{c(r)}{r^3} = c$, $(|c| < \infty)$. $\square$

8. Simulation and Evaluation

8.1. Surface Generation

In order to compare the coverage property of surfaces with different curvatures, we consider the following surfaces which can be expressed as a single valued function $z = h(x, y)$:

$$z = 100 + 50\sin\left(\frac{C\pi x}{1000}\right)\sin\left(\frac{C\pi y}{1000}\right), \tag{30}$$

where $x, y \in [0, 3000]$ m, and the parameter C is taken as $C = 1, 3, 9$ to generate three surfaces with $9, 81$ and 729 peaks and valleys in the region $[0, 3000]\,\text{m} \times [0, 3000]\,\text{m}$, respectively. Fig 5 gives the contours of these surfaces. Here, the unit of length is the meter.

8.2. Numerical Results

The first simulation is implemented in the *FoI* with three different surfaces S given by Equ.(30). $n = 1000$ sensors with the same sensing range $r = 20$m are randomly deployed on the surface according to $SP3$ distribution, and they could independently and randomly move at speed of $v = 1$m/s on the surface.

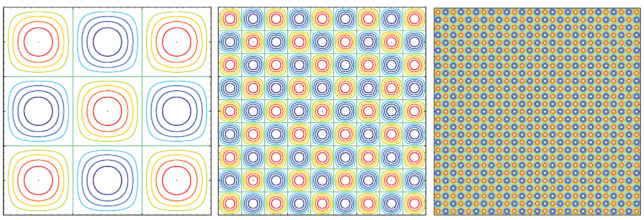

Figure 5: The contours of the surfaces with $9, 81$, and 729 peaks and valleys in a region spanning over a $[0, 3000]\,\text{m} \times [0, 3000]\,\text{m}$ square, respectively.

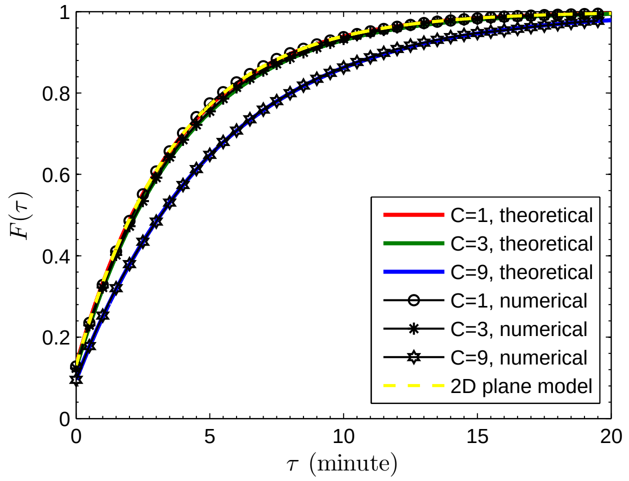

Figure 6: The comparison of coverage ratio over the time interval $[0, \tau)$ ($\tau = 20$ minutes) obtained by the simulation results and theory results. The theoretical and numerical results for the $C = 9$ case overlap, while the rest five lines overlap.

The $SP3$ distribution on the surface could be generated by the Acceptance-Rejection method [37]. To compute the coverage ratio, the region is divided into 3000×3000 cells and the movement is approximated with time step $\Delta t = 0.06s$.

Besides, the theory results presented in Theorem 7.4 for general surface are also applied to evaluate the coverage ratio. Note that the function $h_r(v\tau) = \lim_{n\to\infty} \frac{1}{n}\sum_{i=1}^{n} \int_0^{v\tau} \mathcal{G}_i(k_n, r, s)ds$ is difficult to obtain directly and sensors are deployed uniformly and move randomly. Hence, if n is very large, we can take the following approximation

$$h_r(v\tau) \approx \frac{v\tau}{||S||} \int\int_{p\in S} \left(\frac{1}{2\pi}\int_0^{2\pi} \mathcal{G}(k_n^\theta, r, p)d\theta\right)dp, \tag{31}$$

where k_n^θ denotes the normal curvature at θ–direction, which is given by

$$k_n^\theta(p) = \frac{\left|h_{xx}(p)\cos^2\theta + 2h_{xy}(p)\cos\theta\sin\theta + h_{yy}(p)\sin^2\theta\right|}{\left(1 + (h_x(p)\cos\theta + h_y(p)\sin\theta)^2\right)^{\frac{3}{2}}}.$$

The integral in Equ.(31) need be further approximated by numerical quadrature formulas, such as the trapezoid formula [38].

Fig 6 gives the comparison of coverage ratio over the time interval $[0, \tau)$ ($\tau = 20$ minutes) obtained by the simulation results and theory results. Coverage ratio on 2D region $[0, 3000]$ m $\times$ $[0, 3000]$ m is also shown in Fig 6.

As shown in Fig 6, for the cases of $C = 1, 3, 9$, there is only one theoretical curve when applying the 2D plane model, since the 2D plane model takes into account only the rectangular boundaries of the FoI and ignores the terrain fluctuations within these boundaries. In all there cases, we have the general trend that the coverage ratio increases with the time period. This is consistent with the intuition that "mobility increases the surface coverage", because we have assumed constant speed for

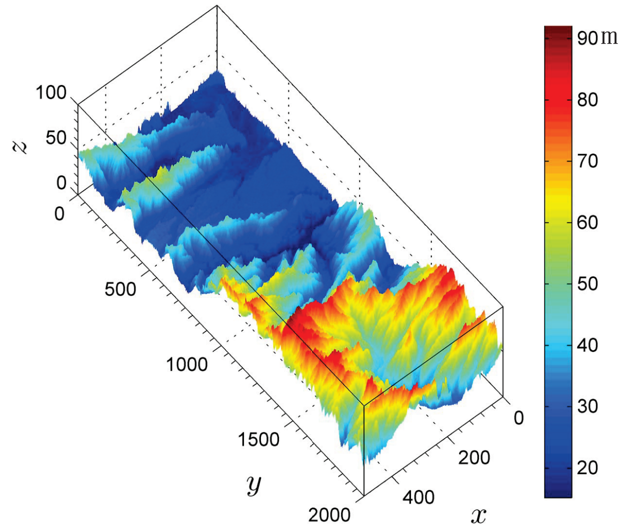

(a) Real-world surface

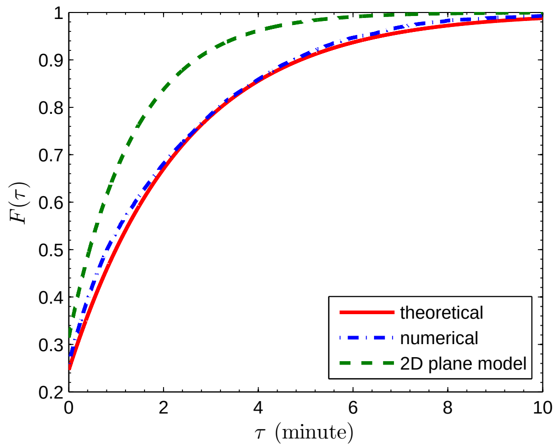

(b) Evaluation results

Figure 7: (a) The real-world surface S taken from the Tianmu Mountain. (b) The comparison of coverage ratio over the time interval $[0, \tau)$ ($\tau = 10$ minutes) obtained by the simulation results and theory results.

convenience and longer time period with constant speed equals to greater speed with constant time period, as given in Remark 3.3. Our theoretical results approximate quite well with the numerical coverage ratio, while for the $C = 9$ case, the numerical results differ from the curve of 2D plane model. This lead us to the conclusion that when the terrain is flat, our results for surface coverage ratios behave comparably with results derived using the 2D plane assumption; however, when the terrain fluctuates, then our results are more accurate.

8.3. Real-world Evaluation

We further perform evaluation on a real world surface, the Tianmu Mountain, which is a mountain in Lin'an County in Northwestern Zhejiang province in eastern China. It has coordinates $30°18'N \sim 30°24'N$ and $119°23'E \sim 119°28'E$. We choose this area because the GreenOrbs sensor network [4], which at present is the largest outdoor real sensor networks with more than one thousand sensor nodes, is deployed there. The corresponding terrain data can be downloaded from the public web site of the *Consortium for Spatial Information (CGIAR-CSI)* [39].

Fig. 7 presents the surface S, a $[0, 500]\,\mathrm{m} \times [0, 2000]\,\mathrm{m}$ region. $n = 300$ sensors with the same sensing range $r = 20$m are randomly deployed on the surface with uniform distribution, and they could independently and randomly move at speed of $v = 1\mathrm{m/s}$ on the surface.

The data of surface are discrete function values but function expression, thus the partial derivatives of function $h(x, y)$ in evaluating k_n^θ need be approximated with difference quotients [38]. Taking $h_{xx}(x_i, y_j)$ as example, i.e.,

$$h_{xx}(x_i, y_j) \approx \frac{h_{i+1,j} - 2h_{i,j} + h_{i-1,j}}{\Delta x^2},$$

where $h_{i,j} = h(x_i, y_j)$ denotes the value of function $h(x, y)$ at the uniform mesh point (x_i, y_j).

Fig 7(b) presents the comparison of coverage ratio over the time interval $[0, \tau)$ ($\tau = 10$ minutes) obtained by the simulation results and theory results. The coverage ratio based on a 2D plane model is also shown in Fig.7(b).

As can be seen clearly from Fig.7(b), the intuition that "mobility increased the surface coverage ratio" holds well. The 2D plane model will give quite optimistic prediction of the surface coverage ratio. This is because the 2D plane model totally ignores the terrain fluctuation. As expected, our theoretical result approximate well with the numerical results. Furthermore, this evaluation taken on real-world surface show that our theoretical results can guide the deployment of mobile sensor network in applications concerning complex sensing fields, e.g., networks designers first download public available terrain data and then follow the numerical process to decide the number of sensors to be deployed.

9. Conclusion and Future Work

In this section, we discuss some practical issues of our models, identify future extensions, and conclude our work.

- *Surface is non-convex.* Our analytical result is derived by modeling the target FoI as a convex surface. However, a real world surface can be more complicated, i.e., it may consist of multiple separate regions due to obstacles (e.g., rocks, trees, lakes, etc.). Combine existing integral and differential geometry results, we will extend the derived results to take these scenarios.

- *The Unit Ball Sensing Model.* The Unit Ball Sensing Model is a simplified model assuming a binary cut-off in a sensor's sensing performance, which is not true in real scenarios. For 2D plane coverage and 3D space coverage, the Quasi Unit Disk model is thus sometimes adopted. There are two critical sensing ranges r_l and r_h, such that the success ratio of sensing an event is 1 for distance smaller than r_l, 0 for distances bigger than r_h and p ($0 < p < 1$) for distances between r_l and r_h. On the one hand, our analysis framework can be easily extended to a quasi unit ball model. On the other hand, the derived results can be revised to get the lower bound of coverage ratio when using the lower sensing ranges r_l, the upper bound of coverage ratio when using the upper sensing range r_h, and the expected coverage ratio when using the estimated expectation of sensing range.

- *The impact of heterogeneity on the surface coverage.* Note that we have assumed the sensors network to be homogeneous. The sensing coverage of a sensor node is usually assumed to be uniform in all directions and is represented by a unit ball model in our work. However, heterogeneity is an inherent property of many applied sensor networks [35]. On 3D surfaces, the corresponding results are unknown when sensing areas of sensors do not follow the unit ball model but can have arbitrary shape and sensors do not have an identical sensing capability.

- *Mobility patterns.* In a mobile sensor network, depending on the mobile platform and application scenario, sensors can choose from a wide variety of mobility strategies, from passive movement to highly coordinated and complicated motion [18]. Sensors deployed in the air or ocean move passively according to external forces, such as air and ocean currents [11], or wild animals [1]; simple robots may have a limited set of mobility patterns, and advanced robots can navigate in a more complicated fashion. Still, sensors can move under arbitrary mobility patterns. In our model, sensors move under the GC Walk which can serve as a bound for mobility in reality [1][2][11]. Furthermore, sensors may move collaboratively instead, the corresponding coverage improvement is unknown.

To summarize, we have studied the surface coverage of mobile sensor networks, with comprehensive consideration of the network configuration, target field's features and sensor's mobility. Specifically, we have investigated the expected area of the region covered by a sensor moves on 2D plane, sphere and general surface. In addition, we have obtained mathematical formulas for the corresponding coverage ratio at one time instant and over a time interval. Our coverage ratio for the 2D plane case and the sphere case are just two special cases of that of the general convex 3D surface case, thus we provide a unified analysis framework. The analysis in this paper shed light on understanding of the invalidity of previous results and the results here are the first trial to characterize the surface coverage with mobile nodes. Finally, simulation and real-world evaluation verify our theoretical results. In the future, we will study more general scenarios of sensor networks with heterogeneous nodes, other sensor distribution and other random mobility patterns. A more interesting issue for future study is the coverage improvement brought about by sensors moving in a collaborative manner.

Acknowledgement

This research was supported by NSF of China (No.61073158, 61100210, 61170238, 60903190, and 61027009), STCSM Project (No.12dz1507400), Doctoral Program Foundation of Institutions of Higher Education (No.20110073120021), Doctoral Fund of Ministry of Education of China (No.20100073120021), National 863 Program (No. 2009AA012201 and 2011AA010500), SJTU SMC Project (No.201120), and Singapore NRF (No.CREATE E2S2).

[1] P. Juang, H. Oki, Y. Wang, M. Martonosi, L.S. Peh, and D. Rubenstein. Energy-efficient computing for wildlife tracking: design tradeoffs and early experiences with ZebraNet. In *Proc. ASPLOS-X*, October 2002.

[2] S. Xing, C. Shahabi, and B. Pan. Continuous monitoring of nearest neighbor on land surface. In *Proc. VLDB*, August 2009.

[3] M. Hefeeda and M. Bagheri. Wireless sensor networks for early detection for forest fires. In *Proc. MASS*, October 2007.

[4] Y. Liu, Y. He, M. Li, J. Wang, K. Liu, L. Mo, W. Dong, Z. Yang, M. Xi, J. Zhao, and X.-Y. Li. Does wireless sensor network scale? A measurement study on greenorbs. In *IEEE INFOCOM*, pages 873-881, April 2011.

[5] G. Werner-Allen, K. Lorincz, J. Johnson, J. Lees, and M. Welsh. Fidelity and yield in a volcano monitoring sensor network. *USENIX Symposium on Operating System Design and Implementation (OSDI)*, 2006.

[6] L. Kong, D. Jiang, and M.-Y. Wu. Optimizing the spatio-temporal distribution of cyber-physical systems for environment abstraction. In *Proc. ICDCS*, June 2010. ACM.

[7] L. Kong, M. Xia, X.-Y. Liu, M.-Y. Wu, X. Liu. Data loss and reconstruction in sensor networks. In *IEEE INFOCOM*, April 2013.

[8] S. Meguerdichian, F. Koushanfar, M. Potkonjak, and M.B. Srivastava. Coverage problems in wireless ad-hoc sensor networks. *IEEE INFOCOM 2001.*, April 2001.

[9] Q. Wang, X. Wang, and X. Lin. Mobility increases the connectivity of k-hop clustered wireless Networks. In *Proc. ACM Mobicom 2009*, September 2009.

[10] Y. Mei, Y.-H. Lu, Y. C. Hu, and C.S.G. Lee. Deployment of mobile robots with energy and timing constraints. *IEEE Transactions on Robotics*, 2006.

[11] J. Luo, D. Wang, and Q. Zhang. Double mobility: coverage of the sea surface with mobile sensor networks. In *IEEE INFOCOM*, 2009.

[12] A. Howard, M. J. Mataric, and G. S. Sukhatme. Mobile sensor network deployment using potential fields: a distributed, scalable solution to the area coverage problem. In *DARS*, 2002.

[13] Y. Zhou and K. Chakrabarty. Sensor deployment and target localization based on virtual forces. *In INFOCOM*, 2003.

[14] G. Wang, G. Cao, and T. L. Porta. Movement-assisted sensor deployment. *In INFOCOM*, 2004.

[15] H. Zhou, H. Wu, S. Xia, M. Jin, and N. Ding. A distributed triangulation algorithm for wireless sensor networks on 2D and 3D surface. *IEEE INFOCOM*, pp.1053-1061, Shanghai, China, April, 2011.

[16] M. Jin, G. Rong, H. Wu, L. Shuai, and X. Guo. Optimal surface deployment problem in wireless sensor networks. *IEEE INFOCOM*, pp.2345-2353, Orlando, March, 2012.

[17] L. Liu, and H. Ma. On coverage of wireless sensor networks for rolling terrains. IEEE Transactions on Parallel and Distributed Systems, 23(1):118C125, 2012.

[18] B. Liu, P. Brass, O. Dousse, P. Nain, and D. Towsley. Mobility improves coverage of sensor networks. *In Proc. MobiHoc*, 2005.

[19] W. Wang, V. Srinivasan, and K.-C. Chua. Trade-off between mobility and density for coverage in wireless sensor networks. In *Proc. MobiCom*, 2007. ACM.

[20] M. Grossglauser and D. Tse. Mobility increases the capacity of ad hoc wireless networks. *IEEE/ACM Transaction on Networking*, vol.10, no.4, pages 477-486, Agugust 2002.

[21] S. Čapkun, J. Hubaux, and L. Buttyán. Mobility helps security in ad hoc networks. In *Porc. ACM MobiHoc 2003*, June 2003.

[22] M.-C. Zhao, J. Lei, M.-Y. Wu, Y. Liu, and W. Shu. Surface coverage in wireless sensor networks. In *IEEE INFOCOM*, April 2009.

[23] L. Kong, M. Zhao, X.-Y. Liu, J. Lu, Y. Liu, M-Y. Wu, and W. Shu. Surface coverage in sensor networks. *IEEE Transactions on Parallel and Distributed Systems*, 2013.

[24] P.-J. Wan and C.-W. Yi. Coverage by randomly deployed wireless sensor networks. *IEEE Transactions on Information Theory*, Vol.52, No.6, June 2006.

[25] X. Bai, Z. Yun, D. Xuan, T. H. Lai, and W. Jia. Optimal patterns for four-connectivity and full-coverage in wireless sensor networks. *IEEE Trans. Mob. Comput.*, 9(3):435-448, 2010.

[26] X. Bai, C. Zhang, D. Xuan, and W. Jia. Full-coverage and k-connectivity (k= 14, 6) three dimensional networks. *IEEE INFOCOM*, April 2009.

[27] P. Balister, B. Bollobas, A. Sarkar, and S. Kumar. Reliable density estimates for coverage and connectivity in thin strips of finite length. In *Proc. MobiCom*, September 2007. ACM.

[28] M. Cardei and J. Wu. Coverage in wireless sensor networks in handbook of sensor networks. *CRC Press*, 2004.

[29] M. Li, W. Cheng, K. Liu, Y. He, X.-Y. Li, and X. Liao. Sweep Coverage with Mobile Sensors. *IEEE Transactions on Mobile Computing*, Vol.10(11), pages 1534-1545, November 2011.

[30] B. Wang. Coverage problems in sensor networks: A survey. ACM Computing Surveys, pages.1-53, 2011.

[31] M.P.do Carmo. Differential geometry of curves and surfaces. *Prentice-Hall, Englewood CLiffs*, N.J., 1976.

[32] R. Serfozo. Introduction to stochastic networks. *Springer*, 1999.

[33] P. Hall. Introduction to the theory of coverage process. *John Wiley & Sons*, 1988.

[34] C.-F. Huang, Y.-C. Tseng, and L.-C. Luo. The coverage problem in three-dimensional wireless sensor networks. *IEEE GLOBECOM*, Nov.-3 Dec. 2004.

[35] X. Wang, X. Wang, and J. Zhao. Impact of mobility and heterogeneity on coverage and energy consumption in wireless sensor networks. In *Proc. ICDCS*, June 2011. ACM.

[36] H. Zhang and J. Hou. Maintaining sensing coverage and connectivity in large sensor networks. *Ad Hoc and Sensor Wireless Networks*, 2005.

[37] J. Banks. Handbook of Simulation: Principles, Methodology, Advances, Applications, and Practice. *John Wiley & Sons*, 1998, p.145-147.

[38] J. Todd. Numerical analysis. *Birkhaüser Verlag*, 1979.

[39] The web site of CGIAR-CSI: http://srtm.csi.cgiar.org/SELECTION/inputCoord.asp

Appendix A. Preliminaries of Integral and Differential Geometry

Supporting mathematical knowledge are: curvatures of curves and surfaces; convex sets. Related definitions are listed here, and the readers can refer to [31] for more detailed explanations.

Definition Appendix A.1. *Surface S is **k-fold continuously differentiable**, i.e., S is in the class $\mathbb{C}^k$, if in some neighborhood of each point on S, it is k-fold continuously differentiable.*

Definition Appendix A.2. *Surface S is **convex** if the Gaussian curvature K at each point of S is nonnegative, i.e., $K(p) \geq 0, \forall p \in S$.*

Definition Appendix A.3. *Curvature of a curve. Let $\mathcal{L}$ be a smooth curve in $\mathbb{R}^3$, take on it a point p and another point p_1. Let Δs denote the arc length of pp_1 on $\mathcal{L}$, $\Delta\theta$ denote the angle between tangent vectors $\overrightarrow{\tau}$ and $\overrightarrow{\tau_1}$ to $\mathcal{L}$ at p and p_1. Let $k = \lim_{p \to p_1} \frac{\Delta\theta}{\Delta s} = \lim_{\Delta s \to 0} \frac{\Delta\theta}{\Delta s}$, if it exists. k is called the curvature of curve $\mathcal{L}$ at point p.*

Definition Appendix A.4. *Normal curvature k_n. At any point on a surface we can find a normal vector which is at right angles to the surface. The intersection of a plane containing the normal with the surface will form a curve called a normal section and the curvature of this curve is the normal curvature.*

Definition Appendix A.5. *Geodesic curvature k_g. For a point on a curve lying on a surface, the curvature of the orthogonal projection of the curve onto the tangent plane to the surface at the point; it measures the departure of the curve from a geodesic.*

Definition Appendix A.6. *Gaussian curvature. For points on different sections of a surface, their will have different normal curvatures; the maximum and minimum values of these are called the principle curvatures, i.e., k_1 and k_2. The Gaussian curvature is the product of the two principle curvatures, i.e., $K = k_1 k_2$.*

Basic information: (a) let $\mathcal{L}$ be a straight line. Then $\Delta\theta = 0$, and thus $k = 0$ holds at every point of $\mathcal{L}$; (b) let $\mathcal{L}$ be a circle of radius R, as $\Delta s = R\Delta\theta$, and thus $\lim_{\Delta s \to 0} \frac{\Delta\theta}{\Delta s} = \frac{1}{R}$, i.e. the curvature of a circle is a constant; (c) the Gaussian curvature is 0 for a plane and $1/R^2$ for a sphee of radius R.

Lemma Appendix A.1. *The curve $\mathcal{L}$ on surface S with curvature of $k(s)$, geodesic curvature of $k_g(s)$ and normal curvature of $k_n(s)$ at $s \in \mathcal{L}$ has the following relation:*

$$k^2(s) = k_g^2(s) + k_n^2(s).$$

Theorem Appendix A.2. *Gauss-Bonnet Theorem. Suppose $G \subseteq S$ is a compact two-dimensional Riemannian manifold with boundary ∂G. If ∂G is piecewise smooth and has n turns, let θ_i be the ith "turning" angle, then we have:*

$$\iint_G KdS + \int_{\partial G} k_g ds + \sum_{i=1}^{n} (\pi - \theta_i) = 2\pi.$$

Lemma Appendix A.3. *If ∂G is a closed smooth curve on S, thus*

$$\iint_G KdS + \int_{\partial G} k_g ds = 2\pi.$$

Definition Appendix A.7. *Surface convex set.*[5] *We call $\mathcal{K}$ (with $\mathcal{K} \subseteq S$) a surface convex set if and only if the geodesic curve between any two points in $\mathcal{K}$ is a subset of $\mathcal{K}$.*

Definition Appendix A.8. *Surface parallel convex set.*[6] *The surface parallel set $\mathcal{K}_\delta$ of $\mathcal{K}$ is defined by*

$$\mathcal{K}_\delta = \bigcup_{x \in \mathcal{K}} \{y \mid y \in S, d(x, y) \leq \delta\}.$$

Set $\mathcal{K}_\delta$ is difined in this paper to takle the boundary effect of set $\mathcal{K}$ as the latter one is not infinite.

[5] On 2D planes, change "geodesic curve" to "line segment".

[6] For 2D planes, substitute S with $\mathbb{R}^2$.

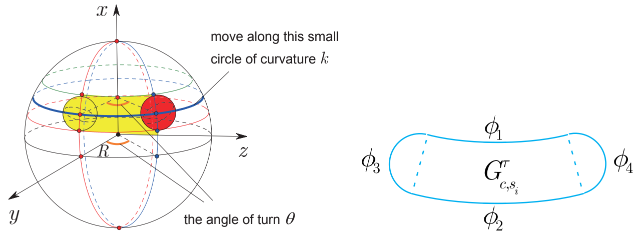

(a) (b)

Figure B.8: Sensor s_i moves on a sphere under CA Walk over $[0, \tau)$; (a) An overview; (b). The region covered by s_i during $[0, \tau)$.

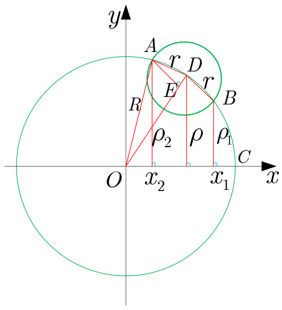

Figure B.9: CA Walk Case: Geometric relations

Definition Appendix A.9. *Diameter of a surface convex set. Given a surface convex set $\mathcal{K}$ on S, let $|\mathcal{K}|_D$ denote the upper bound of the Euclidean distance between any two points in $\mathcal{K}$, which is called the diameter of $\mathcal{K}$ and defined as*

$$|\mathcal{K}|_D = \sup_{\forall x,y \in \mathcal{K}} \left\{ d(x, y) \right\}.$$

Lemma Appendix A.4. *The Z–projection of a point (x, y, z) is the point (x, y) on the corresponding xOy plane. The Z–projection of a surface convex set is a planar convex set.*

Appendix B. Proof of Theorem 6.2

Proof. As shown in Fig B8(a) and Fig B8(b), the curve segments $\phi_1, \phi_2, \phi_3, \phi_4$ on S concatenate each other together and form a closed smooth curve $\partial G^{\tau}_{c,s_i}$. Note that $K = 1/R^2$ and on each curve segment, k_g, ϕ_i) $(1 \leq i \leq 4$, is constant, and $k_g(\phi_3) = k_g(\phi_4)$. Let s_i denote the arc length. From Lemma Appendix A.3, we obtain

$$\begin{aligned}
\left\| G^{\tau}_{c,s_i} \right\| &= \iint_{G^{\tau}_{c,s_i}} dS = R^2 \iint_{G^{\tau}_{c,s_i}} KdS \\
&= R^2 \left(2\pi - \int_{\partial G^{\tau}_{c,s_i}} k_g ds \right) \\
&= R^2 \left(2\pi - \sum_{i=1}^{2} k_g(\phi_i) s_i - k_g(\phi_3)(s_3 + s_4) \right).
\end{aligned} \tag{B.1}$$

We further consider the geometric relations on the cross section xOy (see Fig B9). From Lemma 6.1, we get

$$\begin{gathered}
\left| k_g(\phi_i) \right| s_i = \frac{\sqrt{R^2 - \rho_i^2}}{R\rho_i} \rho_i \theta = \frac{|x_i|}{R} \theta, \\
i = 1, 2, \ k_g(\phi_2) > 0, \ k_g(\phi_1) \ sgn(x_1) < 0.
\end{gathered} \tag{B.2}$$

where function $sgn(x)$ returns the symbol of input x. Since $\sin\angle DAE = \|DE\| / r = r/(2R)$, we have $\|OE\| = R - \|DE\| = R - r^2/(2R)$. Let $\rho_0 =$

$\rho_3 = \rho_4 = \|AE\|$, then

$$
\begin{aligned}
k_g(\phi_3)(s_3+s_4) &= \frac{\sqrt{R^2-\rho_0^2}}{R\rho_0} 2\pi\rho_0 \\
&= \frac{2\pi\sqrt{R^2-\rho_0^2}}{R} = \frac{2\pi\|OE\|}{R} = 2\pi - \frac{\pi r^2}{R^2}.
\end{aligned} \tag{B.3}
$$

Combining Eq.(B.1), Eq.(B.2) and Eq.(B.3), we get

$$\left\|G^\tau_{c,s_i}\right\| = \pi r^2 + R\theta(x_1-x_2) = \pi r^2 + \frac{Rv\tau}{\rho}(x_1-x_2). \tag{B.4}$$

Also we have

$$\begin{cases} x^2+y^2 = R^2, \\ \left(x-\sqrt{R^2-\rho^2}\right)^2 + (y-\rho)^2 = r^2. \end{cases} \tag{B.5}$$

Through removing y, we obtain

$$x^2 - 2x\left(R-\frac{r^2}{2R}\right)\sqrt{1-\left(\frac{\rho}{R}\right)^2} + \left(R-\frac{r^2}{2R}\right)^2 - \rho^2 = 0. \tag{B.6}$$

Applying Viete's theorem, we get the equation of x_1, x_2:

$$
\begin{aligned}
&|x_1-x_2|^2 = (x_1+x_2)^2 - 4x_1x_2 \\
&= 4\left(R-\frac{r^2}{2R}\right)^2\left(1-\left(\frac{\rho}{R}\right)^2\right) - 4\left(\left(R-\frac{r^2}{2R}\right)^2-\rho^2\right) \\
&= \left(\frac{\rho r}{R}\right)^2\left(4-\left(\frac{r}{R}\right)^2\right).
\end{aligned} \tag{B.7}
$$

Then we have:

$$
\begin{aligned}
\left\|G^\tau_{c,s_i}\right\| &= \pi r^2 + \frac{Rv\tau}{\rho}(x_1-x_2) = \pi r^2 + \frac{Rv\tau}{\rho}\cdot\frac{\rho r}{R^2}\sqrt{4R-r^2} \\
&= \pi r^2 + \frac{rv\tau}{R}\sqrt{4R^2-r^2} = \pi r^2 + rv\tau\sqrt{4-Kr^2}.
\end{aligned} \tag{B.8}
$$

□

Appendix C. Proof of Theorem 7.2

Proof. (1) First we consider the stationary scenario on general surface S. The covered region G^0_{c,s_i} is clipped by sphere S_1 and sphere S_2, where S_1 has Gaussian curvature $K_{min} = \min_{p\in S} K(p)$, S_2 has Gaussian curvature $K_{max} = \max_{p\in S} K(p)$. From Remark 4.2, we have

$$\left\|G^0_{c,s_i}\right\| = \pi r^2 + o(r^2). \tag{C.1}$$

(2) Then we consider the extra region Ω^τ_{c,s_i} covered by sensor s_i when moves along a trace. We use the differential and integration method to characterize $\left\|\Omega^\tau_{c,s_i}\right\|$. Let $\mathcal{L}(s)$ $(0 \le s < v\tau)$ denote the trace of s_i, and let's consider a differential curve element $[s, s+ds]$ on $\mathcal{L}(s)$. It can be approximated as an arc element with radius $\rho = 1/k_n(s)$, denoted as γ_0, on an imaginary spherical surface, denoted as S_ρ. The imaginary S_ρ is a spherical surface which is produced by γ_0 rotating around the trace of s_i with radius ρ, as shown in Fig C10(a).
For the surface diameter of the region Ω_{c,s_i} with the curvature at point $\mathcal{L}(s)$ being $\bar{k}_n(s)$. It can be approximately regarded as an arc curve with radius $\bar{\rho} = \frac{1}{\bar{k}_n(s)}$, in terms of $o(r^2)$ approximation. Then, Ω_{c,s_i} along dS is a fraction of S_ρ that lies on the general surface S. The corresponding fraction is $\frac{ds}{2\pi\rho}$, and Ω_{c,s_i} along the curve element $[s, s+ds]$ has area of $dS = S_\rho \frac{ds}{2\pi\rho}$.
According to the geometric relationship in Fig.B10(b), the arc γ_0 has the mathematical equation

$$y = \rho - \bar{\rho} + \sqrt{\bar{\rho}^2 - x^2}, (x \in [-\delta, \delta]). \tag{C.2}$$

where $\delta = \frac{r}{2}\sqrt{4-(\bar{k}_n(s)r)^2}$.

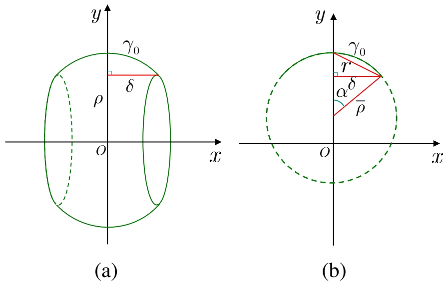

Figure C.10: (a) The imaginary spherical surface by rotating the elementary arc around a sensor's the trace. (b) The geometric relations for the elementary arc on the imaginary spherical surface.

With Equ.(C.2), the area of the revolution surface can be obtained

$$
\begin{aligned}
S_\rho &= 2\pi\int_{-\delta}^{\delta} |y|\sqrt{1+(y')^2}dx \\
&= 2\pi\int_{-\delta}^{\delta}\left(\rho-\bar{\rho}+\sqrt{\bar{\rho}^2-x^2}\right)\frac{\bar{\rho}}{\sqrt{\bar{\rho}^2-x^2}}dx \\
&= 4\pi\bar{\rho}\left[\delta + (\rho-\bar{\rho})\int_0^{\delta}\frac{dx}{\sqrt{\bar{\rho}^2-x^2}}\right] \\
&= 4\pi\bar{\rho}\left[\delta + (\rho-\bar{\rho})arcsin\frac{\delta}{\bar{\rho}}\right] = 4\pi\bar{\rho}\left[\delta+(\rho-\bar{\rho})\alpha\right] \\
&= 4\pi\bar{\rho}\left[\delta + 2(\rho-\bar{\rho})arcsin\frac{r}{2\bar{\rho}}\right]
\end{aligned} \tag{C.3}
$$

By integration of dS, we get

$$
\begin{aligned}
\left\|\Omega^\tau_{c,s_i}\right\| &= \int_0^{v\tau} S_\rho\frac{ds}{2\pi\rho} = 2\int_0^{v\tau}\frac{\bar{\rho}}{\rho}\left[\delta + 2(\rho-\bar{\rho})arcsin\frac{r}{2\bar{\rho}}\right]ds \\
&= \int_0^{v\tau}\mathcal{G}_i(k_n, r, s)ds.
\end{aligned} \tag{C.4}
$$

where $\mathcal{G}_i(k_n, r, s)$ is given by

$$
\begin{aligned}
&\mathcal{G}_i(k_n, r, s) \\
&= \frac{k_n(s)}{\bar{k}_n(s)}\left(r\sqrt{4-(\bar{k}_n(s)r)^2} + 4\frac{\bar{k}_n(s)-k_n(s)}{\bar{k}_n(s)k_n(s)}arcsin\left(\frac{\bar{k}_n(s)r}{2}\right)\right).
\end{aligned} \tag{C.5}
$$

Thus over time interval $[0, \tau)$, the total area covered by a sensor moving along a general curve on general surfaces is

$$\left\|G^\tau_{c,s_i}\right\| = \left\|G^0_{c,s_i}\right\| + \left\|\Omega^\tau_{c,s_i}\right\| = \pi r^2 + \int_0^{v\tau}\mathcal{G}_i(k_n, r, s)ds + o(r^2). \tag{C.6}$$

□

Appendix D. Proof of Theorem 7.3

Proof. Let $\delta = \sup_{\mathcal{K}\subseteq S}\|\mathcal{K}\|_D$. Utilizing rules of clipping and approaching, we obtain the lower bound and then the upper bound.
(1) The lower bound. Since $\mathcal{U}\cap\mathcal{K} \ne \emptyset$, then $\mathcal{K} \subseteq \mathcal{U}_\delta$, and thus

$$
\begin{aligned}
&\mathcal{P}(p\in\mathcal{U}\cap\mathcal{K}|p\in\mathcal{U}, \mathcal{U}\cap\mathcal{K}\ne\emptyset) \\
&\ge \mathcal{P}(\mathcal{U}\cap\mathcal{K}\ne\emptyset|\mathcal{K}\subseteq\mathcal{U}_\delta)\cdot\mathcal{P}(p\in\mathcal{U}\cap\mathcal{K}|p\in\mathcal{U}, \mathcal{U}\cap\mathcal{K}\ne\emptyset) \\
&\ge \mathcal{P}(p\in\mathcal{U}\cap\mathcal{K}|p\in\mathcal{U}, \mathcal{K}\subseteq\mathcal{U}_\delta) \\
&\ge \frac{\|\mathcal{K}\|}{\|\mathcal{U}_\delta\|}.
\end{aligned} \tag{D.1}
$$

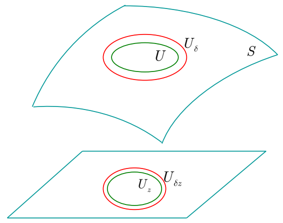

Figure D.11: The surface parallel sets $\mathcal{U}, \mathcal{U}_\delta$ and the corresponding z-projections $\mathcal{U}_z, \mathcal{U}_{\delta z}$.

In order to get the upper bound of $\|\mathcal{U}\|_\delta$, we use $\mathcal{U}_z$ and $\mathcal{U}_{\delta z}$ to denote the z-projection of $\mathcal{U}$ and $\mathcal{U}_\delta$, respectively, on the plane xOy, and $\mathcal{U}_{z\delta}$ to denote the surface parallel set of $\mathcal{U}_z$, as shown in Fig DC11. Then

$$
\begin{aligned}
\|\mathcal{U}\|_\delta &= \iint_{\mathcal{U}_{\delta z}} \sqrt{1 + \| \nabla h\|^2} dxdy \\
&= \iint_{\mathcal{U}_{\delta z} \setminus \mathcal{U}_z} \sqrt{1 + \| \nabla h\|^2} dxdy + \|\mathcal{U}\| \\
&= \sqrt{1 + \|\nabla h\|^2}\Big|_{(x,y)=(\zeta,\eta)} \iint_{\mathcal{U}_{\delta z} \setminus \mathcal{U}_z} dxdy + \|\mathcal{U}\| \\
&\leq M\|\mathcal{U}_{\delta z} \setminus \mathcal{U}_z\| + \|\mathcal{U}\| \leq M\|\mathcal{U}_{z\delta} \setminus \mathcal{U}_z\| + \|\mathcal{U}\| \\
&= \|\mathcal{U}\| + M(\|\mathcal{U}_{z\delta}\| - \|\mathcal{U}_z\|) \\
&= \|\mathcal{U}\| + M\left[(\|\mathcal{U}_z\| + \|\partial \mathcal{U}_z\|\delta + \pi\delta^2) - \|\mathcal{U}_z\|\right] \\
&= \|\mathcal{U}\| + M(\|\partial \mathcal{U}_z\|\delta + \pi\delta^2).
\end{aligned}
\tag{D.2}
$$

where $A \setminus B$ means that set A subtracts set B. Therefore, we have:

$$
\mathcal{P}(p \in \mathcal{U} \cap \mathcal{K} | p \in \mathcal{U}, \mathcal{U} \cap \mathcal{K} \neq \emptyset) \geq \frac{\|\mathcal{K}\|}{\|\mathcal{U}\| + M(\|\partial \mathcal{U}_z\|\delta + \pi\delta^2)}. \tag{D.3}
$$

(2) The upper bound. In fact,

$$
\begin{aligned}
&\mathcal{P}(p \in \mathcal{U} \cap \mathcal{K} | p \in \mathcal{U}, \mathcal{U} \cap \mathcal{K} \neq \emptyset) \\
&\leq \mathcal{P}(p \in \mathcal{U} \cap \mathcal{K} | p \in \mathcal{U}, \mathcal{K} \subseteq \mathcal{U}) \\
&= \mathcal{P}(p \in \mathcal{K} | p \in \mathcal{U}, \mathcal{K} \subseteq \mathcal{U}) = \frac{\|\mathcal{K}\|}{\|\mathcal{U}\|}.
\end{aligned}
\tag{D.4}
$$

Hence, the theorem is proved. □

Mobility Increases the Surface Coverage of Distributed Sensor Networks

Xiao-Yang Liu[a*], Kai-Liang Wu[b], Yanmin Zhu[a], Linghe Kong[a], Min-You Wu[a]

[a]*Department of Computer Science and Engineering, Shanghai Jiao Tong University, Shanghai, China*

[b]*School of Mathematical Science, Peking University, Beijing, China*

[**]Corresponding author

Email addresses: yanglet@sjtu.edu.cn (Xiao-Yang Liu[a*]), wukl@pku.edu.cn (Kai-Liang Wu[b]), yzhu@sjtu.edu.cn (Yanmin Zhu[a]), linghe.kong@sjtu.edu.cn (Linghe Kong[a]), mwu@sjtu.edu.cn (Min-You Wu[a])